SCISPACE
formerly Typeset

Open access • Journal Article • DOI:10.1049/IET-OPT:20070030

# Free-space optical communication employing subcarrier modulation and spatial diversity in atmospheric turbulence channel — Source link

Wasiu O. Popoola, Zabih Ghassemlooy, Joe Allen, Erich Leitgeb ...+1 more authors

**Institutions:** Northumbria University, Graz University of Technology

**Published on:** 22 Feb 2008 - Iet Optoelectronics (Institution of Engineering and Technology)

**Topics:** Subcarrier, Antenna diversity, Phase-shift keying, Demodulation and Modulation

Related papers:

- BPSK Subcarrier Intensity Modulated Free-Space Optical Communications in Atmospheric Turbulence
- Free-space optical communication through atmospheric turbulence channels
- Mathematical model for the irradiance probability density function of a laser beam propagating through turbulent media
- Optical wireless links with spatial diversity over strong atmospheric turbulence channels
- Optical Communication Using Subcarrier PSK Intensity Modulation Through Atmospheric Turbulence Channels

Share this paper:

View more about this paper here: https://typeset.io/papers/free-space-optical-communication-employing-subcarrier-4dxrbht4gd

Northumbria Research Link

Citation: Popoola, Wasiu Oyewole, Ghassemlooy, Zabih, Allen, Joe, Leitgeb, Erich and Gao, Steven (2008) Free-space optical communication employing subcarrier modulation and spatial diversity in atmospheric turbulence channel. IET Optoelectronics, 2 (1). pp. 16-23. ISSN 1751-8768

Published by: IET

URL: http://dx.doi.org/10.1049/iet-opt:20070030 <http://dx.doi.org/10.1049/iet-opt:20070030>

This version was downloaded from Northumbria Research Link: http://nrl.northumbria.ac.uk/id/eprint/1766/

Northumbria University has developed Northumbria Research Link (NRL) to enable users to access the University's research output. Copyright © and moral rights for items on NRL are retained by the individual author(s) and/or other copyright owners. Single copies of full items can be reproduced, displayed or performed, and given to third parties in any format or medium for personal research or study, educational, or not-for-profit purposes without prior permission or charge, provided the authors, title and full bibliographic details are given, as well as a hyperlink and/or URL to the original metadata page. The content must not be changed in any way. Full items must not be sold commercially in any format or medium without formal permission of the copyright holder. The full policy is available online: http://nrl.northumbria.ac.uk/policies.html

This document may differ from the final, published version of the research and has been made available online in accordance with publisher policies. To read and/or cite from the published version of the research, please visit the publisher's website (a subscription may be required.)

Northumbria University NEWCASTLE

UniversityLibrary

# Free-space optical communication employing subcarrier modulation and spatial diversity in atmospheric turbulence channel

W.O. Popoola, Z. Ghassemlooy, J.I.H. Allen, E. Leitgeb and S. Gao

**Abstract:** An expression for the bit error rate of a multiple subcarrier intensity-modulated atmospheric optical communication system employing spatial diversity is derived. Spatial diversity is used to mitigate scintillation caused by atmospheric turbulence, which is assumed to obey log-normal distribution. Optimal but complex maximum ratio, equal gain combining (EGC) and relatively simple selection combining spatial diversity techniques in a clear atmosphere are considered. Each subcarrier is modulated using binary phase shift keying. Laser irradiance is subsequently modulated by a subcarrier signal, and a direct detection PIN receiver is employed (i.e. intensity modulation/direction detection). At a subcarrier level, coherent demodulation is used to extract the transmitted data/information. The performance of on–off-keying is also presented and compared with the subcarrier intensity modulation under the same atmospheric conditions.

## 1 Introduction

Free-space optical (FSO) communications have been the focus of growing research activities as an alternative – or even the ultimate solution – to the access network bottleneck. The increasing research in FSO is spurred by its successful commercial deployments [1]. The capacity of FSO is comparable with that of an optical fibre-based system but at relatively low cost; it requires less time to deploy, is re-deployable (no sunk cost) and is more environmentally friendly as it requires no digging of trenches or cutting of roads and rights of way [2, 3]. FSO finds application in a number of areas such as the cellular communication back haul, optical fibre communication (in the form of redundant links), exhibition halls and disaster recovery among other emerging applications [4, 5]. Of primary concern in FSO, however, is the dependence of the channel on weather which, unfortunately, is not of fixed characteristics, unlike optical fibre-based systems [2, 6]. Effects of fog, rain, atmospheric gases and aerosols result in beam attenuation because of photon absorption (extinguishing of photons) and scattering (change in the direction of photons) [7, 8]. Strong wind and building sway also result in performance degradation and the background radiations from both natural and artificial sources add to the system noise level [9]. There is also a safety requirement that limits the allowable laser power transmitted.

Furthermore, shape, direction and electromagnetic properties of a laser beam are affected by atmospheric turbulence [7]. Turbulence is due to random changes in the refractive index of the atmosphere, an effect that results from a combination of randomly varying temperature, wind speed and pressure. In a clear atmosphere, attenuation coefficient is considered to be low and turbulence becomes the main source of impairment in long-range (over 1 km) FSO links [10]. The turbulence-induced fading (scintillation) in the clear atmosphere can be circumvented through aperture averaging, robust error control coding and diversity techniques. For aperture averaging, the receiver aperture needs to be far greater than the spatial coherence distance $\rho_o$ of the atmospheric turbulence. This condition is not always achievable in FSO as the spatial coherence distance is of the order of centimetres [10]. For coding to be effective in FSO, it needs to be robust to detect/correct burst errors as well as random errors. This is mainly due to the temporal coherence time $\tau_0$ of atmospheric turbulence, which is much greater than the symbol duration $T$. In this work receiver (spatial) diversity is considered as a means of circumventing scintillation. In addition, binary phase shift keying (BPSK)-based subcarrier intensity modulation (SIM) is employed to avoid the need for adaptive threshold required by optimum on–off–keying (OOK). Moreover, SIM has the capability to increase the system capacity by modulating multiple digital and/or analogue information sources onto different electrical subcarriers, which are then used to modulate the intensity of a continuous wave laser that serves as the optical carrier. This, however, comes at the price of increased signal-to-noise ratio (SNR) at a given level of bit error rate (BER) performance. Hence, multiple SIM can only be used when increased capacity is of paramount importance over power requirement. This technique (also termed multiple carriers in ratio frequency (RF)) has been successful in RF communications, has been deployed in many applications such as digital TV, local area networks (LANs), asymmetric digital subscriber line (ADSL) and 4G communications and has already found its way into the optical fibre communication systems [11, 12].

At the receiver end, direct detection using PIN photodetectors is adopted and the laser beam intensity fluctuation in weak turbulence is modelled as a log-normal distribution.

© The Institution of Engineering and Technology 2008

doi:10.1049/iet-opt:20070030

Paper first received 10th April and in revised form 10th July 2007

W.O. Popoola, Z. Ghassemlooy, J.I.H. Allen and S. Gao are with Northumbria Communication Research Lab (NCRLab), Northumbria University, Newcastle upon Tyne, UK

E. Leitgeb is with Institute of Broadband Communications, Graz, TU, Austria

E-mail: wasiu.popoola@unn.ac.uk

The channel noise (shot, background radiation and thermal) is modelled as an additive white Gaussian noise with the background radiation being the dominant source [13]. The link is assumed to be basically a line-of-sight with no multipath; hence inter-symbol interference (ISI) is not considered. The rest of the paper is arranged as follows: a weak turbulence model is discussed in Section 2, OOK is discussed in Section 3 for completeness and a comparison with subcarrier modulation discussed in Section 4. Finally, the spatial diversity and conclusions are presented in Sections 5 and 6, respectively.

## 2 Log-normal turbulence model

Atmospheric turbulence results from random fluctuation of the atmospheric refractive index $n$ along the path of a wave traversing the atmosphere. This refractive index fluctuation is the direct product of random variations in atmospheric temperature from point to point [7]. The random temperature changes are a function of altitude and wind speed. The interaction between the laser beam and the turbulent medium results in random amplitude and phase variations (fading) of the information-bearing laser beam – an effect referred to as scintillation [7]. This scintillation causes impairment and performance degradation for long-range ($\simeq$1 km and above) atmospheric optical communication link length [10]. The relationship between the temperature of the atmosphere and its refractive index variation is given by

$$n = 1 + 77.6(1 + 7.52 \times 10^{-3}\lambda^{-2})\frac{P}{T} \times 10^{-6} \quad (1)$$

where $P$ is the atmospheric pressure in millibars, $T$ the temperature in kelvin and $\lambda$ the wavelength in micro metres [14].

Turbulence is usually modelled based on a 'frozen-in' premise [14]. This premise assumes that turbulent eddies are fixed and vary only with the wind speed in some way. It goes on to imply that the temporal variation in statistical properties of the turbulent atmosphere is caused by the airmass movement [14]. The smallest eddy size $l_0$ is called the turbulence inner scale, with a value of a few millimetres, whereas the largest eddy size $L_0$, termed outer scale of turbulence, has its value running to several metres [10].

The effect of turbulence of concern is the intensity fluctuation of laser light traversing the atmosphere-scintillation. The strength of wave amplitude fluctuation in a turbulent medium is given by the variance of log amplitude $X$ (also called the Roytov parameter $\sigma_X^2$) and the transverse coherence length of turbulence $\rho_o$, which are given by (2) and (3), respectively [14]

$$\sigma_X^2 = 0.307C_n^2K^{7/6}L^{11/6} \quad (2)$$

$$\rho_0 \simeq \sqrt{\lambda L} \quad (3)$$

These equations are valid for $l_0 \leq \sqrt{\lambda L} \leq L_0$, where $L$ is the FSO link range, $C_n^2$ the refractive index structure constant (which characterises the strength of refractive index variation in the medium) and $K = 2\pi/\lambda$ the wave number.

Considering that single scattering characterised weak turbulence and assuming that the log intensity $l$ of laser light traversing the turbulent atmosphere to be normally distributed (i.e. $l \sim N(-\sigma_l^2/2, \sigma_l^2)$, the probability density function (pdf) of light intensity $I = I_0 \exp(l)$ is given by [14]

$$p_I(I) = \frac{1}{\sqrt{2\pi}\sigma_l}\frac{1}{I}\exp\left\{-\frac{(\ln(I/I_0) + \sigma_l^2/2)^2}{2\sigma_l^2}\right\} \quad I \geq 0 \quad (4)$$

where $I_0$ is the received intensity without turbulence. Note that in (4), $\sigma_l^2 = 4\sigma_x^2$ and we have assumed that $E[I] = I_0$ to obtain $E[l] = -\sigma_l^2/2$ [15].

The normalised variance of the intensity $\sigma_N^2$ is derived as follows

$$\sigma_N^2 = \frac{E[I^2] - (E[I])^2}{I_0^2} = \exp(\sigma_l^2) - 1 \quad (5)$$

The turbulence model discussed thus far is valid for the weak turbulence with small values of $\sigma_l^2$. For $\sigma_l^2 \geq 1.2$, saturation sets in and the model no longer holds [14]. Further details of turbulence can be found in [10, 14–16] and references therein.

## 3 OOK modulation

In OOK, a digital data bit $d(t) = \{0\}$ is transmitted as an absence of light pulse and $d(t) = \{1\}$ as a pulse of finite duration. OOK is well studied and is known for its simplicity but requires an adaptive threshold to perform optimally in a turbulent atmosphere [10].

### 3.1 Error probability (adaptive threshold) with scintillation

Here, we assume that the receiver has no prior knowledge of the instantaneous atmospheric scintillation, but is acquainted with its statistics. Without loss of generality, we normalise the receiver area to unity such that optical power can henceforth be represented by the optical intensity $I$. If $R$ represents the responsivity of the PIN photodetector, the generated photocurrent is given by

$$i_r(t) = RI + n(t) \quad (6)$$

where $n(t) \sim N(0, \sigma^2)$ is the additive noise.

The marginal probabilities below are obtained by averaging the conditional pdf of $i_r(t)$ over the scintillation statistics. Note that scintillation does not have any effect when no pulse was transmitted

$$P(i_r/0) = \frac{1}{\sqrt{2\pi\sigma^2}}\exp\left(\frac{-i_r^2}{2\sigma^2}\right) \quad (7)$$

$$P(i_r/0) = \int_0^\infty P(i_r/1, I)P_I(I)\,\mathrm{d}I = \int_0^\infty \frac{1}{\sqrt{2\pi\sigma^2}}\exp\left\{-\frac{(i_r - RI)^2}{2\sigma^2}\right\}\frac{1}{\sqrt{2\pi\sigma_l^2}}\frac{1}{I} \exp\left\{\frac{-(\ln(I/I_0) + \sigma_l^2/2)^2}{2\sigma l^2}\right\}\mathrm{d}I \quad (8)$$

Using the optimal maximum a posteriori (MAP) symbol-by-symbol detection with equiprobable OOK data [17], $d(t)$ is decoded as $\hat{d}(t) = \overset{\arg\max}{d} P(i_r/d(t))$ and the

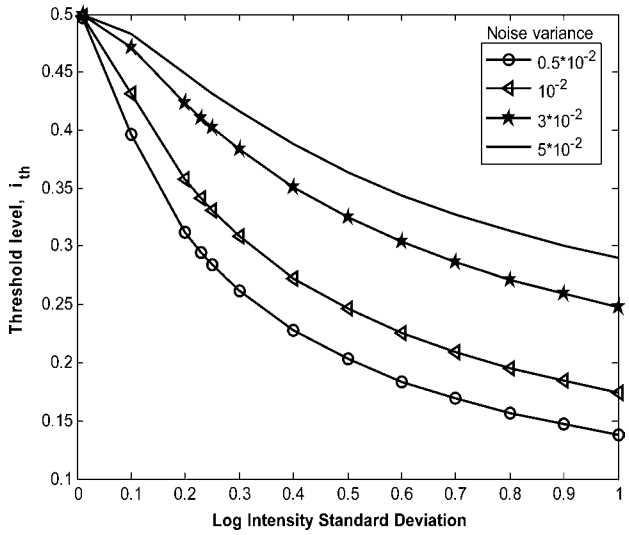


**Fig. 1** *OOK threshold level against the log intensity standard deviation for a range of turbulence levels*

likehood function is given by

$$\Lambda = \int_0^{\infty} \exp\left\{\frac{-((i_r - RI)^2 - i_r^2)}{2\sigma^2}\right\} \frac{1}{\sqrt{2\pi\sigma_l^2}} \frac{1}{I} \exp\left\{\frac{-(\ln(I/I_0) + \sigma_l^2/2)^2}{2\sigma_l^2}\right\} \mathrm{d}I \tag{9}$$

The threshold level, *i*th is obtained from (9) with $\Lambda = 1$. The plot of *i*th for different levels of turbulence with $R$ and $I_0$ both normalised to unity is shown in Fig. 1. This figure clearly illustrates the dynamism in the OOK threshold level. The receiver must therefore be able to select the threshold point adaptively for the optimal performance. Implementation of this is not trivial and we therefore consider SIM as an alternative in the section that follows. The threshold is, however, observed to approach a value of 0.5 as the scintillation level decreases.

The probability of bit error $P_e$ can be obtained from (10)

$$P_e = P(0)\int_{i_{th}}^{\infty} P(i_r/0)\mathrm{d}i_r + P(1)\int_0^{i_{th}} P(i_r/1)\mathrm{d}i_r \tag{10}$$

## 4 Subcarrier modulation

In optical communication systems, SIM is achieved by modulating a digital and/or analogue information source onto an electrical subcarrier, which is in turn used to modulate the intensity of a continuous wave laser that serves as the optical carrier [8, 11, 18]. Information from different sources can also be pre-modulated on different subcarrier signals at different but orthogonal frequencies in multiple SIM (Fig. 2). Optical SIM inherently benefits from more mature RF devices and advances in signal processing. These factors make the implementation of SIM easier, compared with the optimum OOK with adaptive threshold discussed in Section 3. Although the terrestrial FSO link under consideration is assumed horizontal and the channel non-dispersive, SIM is also advantageous in a multipath/dispersive channel. With sufficient number of subcarriers to attain a higher or same overall data rate as a single carrier system, the overall symbol interval of SIM can be made significantly larger than the multipath/dispersive channel delay spread by transmitting at sufficiently low data/symbol rate on each subcarrier [19]. This results in arbitrarily small ISI and eliminates the need for an equaliser.

In addition, subcarrier multiplexing or multiple SIM can be achieved by modulating multiple digital and/or analogue information sources onto different electrical subcarriers, which are then used to modulate the intensity of a continuous wave laser that serves as the optical carrier. Multiple SIM obviously demands tight synchronisation at the receiver side with a major drawback being its poor power efficiency [11, 18, 20]. This results from the fact that the multiple SIM electrical signal is a sum of modulated sinusoids (i.e. dealing with both negative and positive values) and as the intensity of an optical carrier can never be negative, a DC bias $b_o$ is therefore added to this composite signal before it is used to modulate the laser diode intensity. As the number of subcarriers rises, the minimum value of the multiple SIM electrical signal decreases and the required DC bias increases. This factor places a bound on the allowable number of subcarriers for a given peak optical power. However, different approaches have been proposed to alleviate the poor power efficiency, see [11, 18, 20] and references therein. Multiple SIM power efficiency improvement will therefore not be discussed here.

### 4.1 Subcarrier generation and detection

Fig. 2 depicts the block diagram of an FSO system employing subcarrier modulation scheme.

The instantaneous photocurrent $i_r(t)$ is expressed as [8]

$$i_r(t) = RI\,(1 + \beta m(t)) + n(t) \tag{11}$$

where $I = I_{peak}/2$, $I_{peak}$ the peak received irradiance, $\beta$ the modulation index, $m(t)$ the multiple subcarrier signals and $n(t) \sim N(0,\ \sigma^2)$ the additive noise. For $M$ subcarriers,

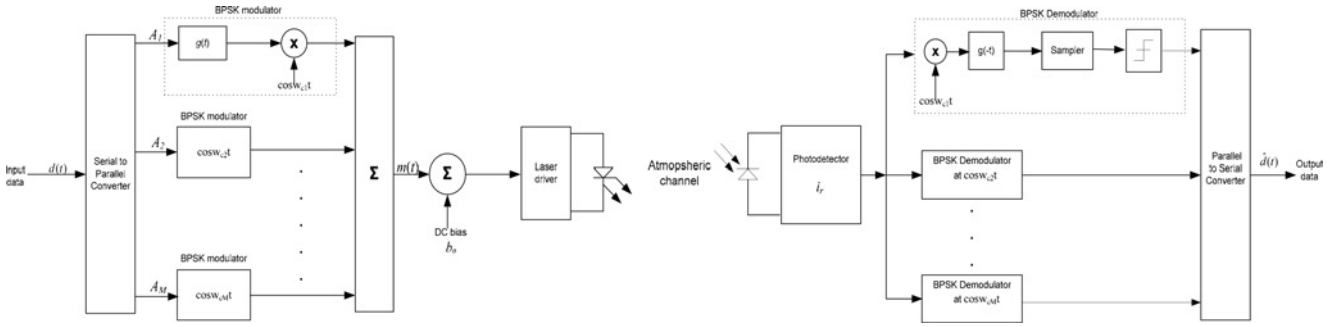


**Fig. 2** *Block diagram of FSO employing SIM*

$m(t)$ over one symbol duration is given by

$$m(t) = \sum_{j=1}^{M} A_j g(t) \cos(w_{cj} t + \theta_j) \tag{12}$$

$$g(t) = \begin{cases} 1 & 0 \le t \le T \\ 0 & \text{elsewhere} \end{cases} \tag{13}$$

where $g(t)$ is the rectangular pulse shape function, $\{w_{cj}\}_{j=1}^{M}$ the angular frequency and $\{A_j\}_{j=1}^{M}$ the peak amplitude of each subcarrier. For a continuous wave laser transmitter to operate within its dynamic range, $|\beta m(t)| \le 1$. Throughout this work, BPSK is assumed on each subcarrier. With $A_j = A$ and $\beta$ normalised to unity, the peak amplitude $A \le 1/M$. The photocurrent for each subcarrier with filtered out DC component and $\theta_j = \{0, \pi\}$ is given by

$$i_r(t) = \pm \mathrm{IRA} g(t) \cos(w_c t) + n(t) \tag{14}$$

The electrical SNR ($\mathrm{SNR_e}$), $\gamma$, at the input of the subcarrier demodulator can be derived from (14) as

$$\gamma = \frac{(\mathrm{IRA})^2}{2\sigma^2} \tag{15}$$

For a fixed value of $\beta$, increasing $M$ will result in reduced SNR as $A \le 1/M$ and subsequently higher BER. In the case of coherent demodulator, the bandpass filter must have twice the transmitted signal bandwidth as made evident by (14).

### 4.2 Error probability (no spatial diversity)

For a coherent BPSK demodulator, the probability of bit error conditioned on the intensity fluctuation can be derived as

$$P_{\mathrm{ec}} = Q\left(\sqrt{\gamma}\right) \tag{16}$$

Averaging (16) over intensity fluctuation statistics results in the following unconditional BER $P_{\mathrm{e}}$

$$P_{\mathrm{e}} = \int_0^{\infty} Q\left(\sqrt{\gamma}\right) \frac{1}{\sqrt{2\pi}\sigma_l^2} \frac{1}{I} \exp\left\{\frac{-(\ln(I/I_0) + \sigma_l^2/2)^2}{2\sigma_l^2}\right\} \mathrm{d}I \tag{17}$$

A closed-form solution of (17) does not exist and could result in truncating the upper limit using the numerical integration. The presence of the argument of the $Q$-function at the lower limit of the integral poses analytical problems [21]. By using an alternative representation of the $Q$-function (18) together with the Gauss–Hermite quadrature integration (19), these problems can be circumvented. See [21] and [22] for further details of (18) and (19), respectively

$$Q(y) = \frac{1}{\pi} \int_0^{\pi/2} \exp\left(-\frac{y^2}{2\sin^2\theta}\right) \mathrm{d}\theta \tag{18}$$

$$\int_{-\infty}^{\infty} f(x) \exp(-x^2)\, \mathrm{d}x \cong \sum_{i=1}^{m} w_i f(x_i) \tag{19}$$

where $\{x_i\}_{i=1}^{m}$ and $\{w_i\}_{i=1}^{m}$ represent the zeros of the $m$th order Hermite polynomial $\mathrm{He}_n(x)$ and the corresponding weight factors, respectively. The degree of accuracy of (19) is determined by the value of $m$. Invoking a change in variable $y = (\ln(I/I_0) + \sigma_l^2/2)/\sqrt{2}\sigma_l$ in (17) and combining this with (18) and (19), we derive the unconditional BER as

$$P_{\mathrm{e}} \cong \frac{1}{\pi} \int_0^{\pi/2} \frac{1}{\sqrt{\pi}} \sum_{i=1}^{m} w_i \exp\left(-\frac{K^2 \exp\left(2(\sqrt{2}\sigma_l x_i - \sigma_l^2/2)\right)}{2\sin^2\theta}\right) \mathrm{d}\theta$$

$$\cong \frac{1}{\sqrt{\pi}} \sum_{i=1}^{m} w_i Q\left(K \mathrm{e}^{(x_i\sqrt{2}\sigma_l - \sigma_l^2/2)}\right) \tag{20}$$

where $K = RI_0A/\sqrt{2}\sigma$. It should be noted that $x_i$ and $w_i$ terms in (20) are independent of $\theta$.

Fig. 3 shows the BER performance against the SNR obtained using (20) and (17) for $m = 20$. There is an excellent agreement between the results, but the Gauss–Hermite quadrature integration (20) is preferred for its compactness and relative simplicity.

## 5 Subcarrier modulation with spatial diversity

We assume the receivers' spatial separation, $s > \rho_{\mathrm{o}}$, resulting in each detector receiving independent signals; $\rho_{\mathrm{o}}$ being of the order of a few centimetres' [14] makes this assumption realistic. However, the use of detector diversity in terrestrial atmospheric optical communication comes with the price of complex tracking and alignment – especially in the presence of building sway and strong winds [9]. We also assumed that the laser radiation to be diffraction-limited and that the beamwidth at the receiver end is sufficiently broad to cover the entire field of view of all the $N$-detectors. The $N$-detector photocurrents $\{i_{ri}(t)\}_{i=1}^{N}$ (Fig. 4) are combined before being sent to the coherent demodulator that separates the composite signal into its constituent subcarriers and demodulates each subcarrier. Spatial diversity combining techniques considered are the maximum ratio combining (MRC), the equal gain combining (EGC) and the selection combining (SelC).

Scintillation, being a random phenomenon that changes with time, makes the received signal intensity to also be time variant with coherence time $\tau_0$ of the order of milliseconds [13]. However, within time duration $t < \tau_0$, the received signal intensity is presumably constant and time invariant. With the symbol duration $T \ll \tau_0$ ($T = 1$ ns when transmitting at a moderate 1 Gbps symbol rate) it

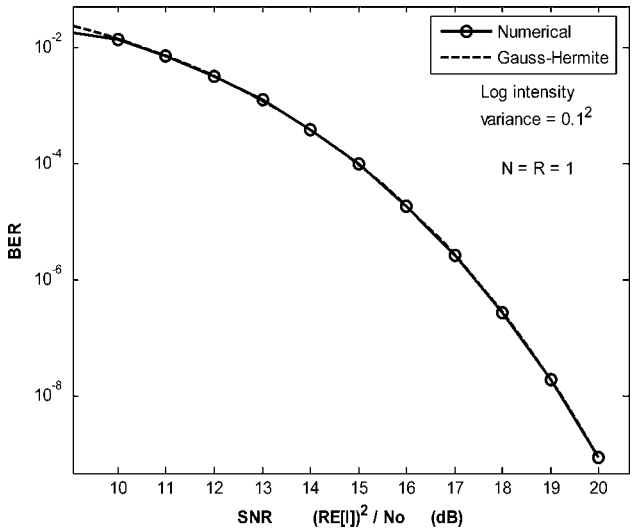


**Fig. 3** *BER against SNR; Numerical and Gauss–Hermite approach solutions for $m = 20$*

follows therefore that the received signal intensity $\{I_i\}_{i=1}^N$ is time invariant over one symbol duration.

To facilitate a fair comparison between the single transmitter–single receiver-system (SISO) and the spatial diversity system, aperture area of each detector in the $N$-receiver system is assumed to be $A_D/N$, where $A_D$ is the aperture area of detector under single transmitter–single receiver link. It follows therefore that the background radiation noise on each link with detector diversity is also $N^{-1}$th that of a SISO link resulting in $\{n_i(t)\}_{i=1}^N \sim N(0, \sigma_i^2/N)$. This approach is particularly valid for the case where noise from the background radiation is the dominant source as is the case for FSO [13]. However, for a thermal noise-limited system, the noise level on each photodetector is not reduced by a factor $N$ but remains constant. By assuming identical PIN photodetector on each link, the individual detector output is given by

$$i_{ri}(t) = \frac{R}{N} I_i \left(1 + \sum_{j=1}^{M} A_j g(t) \cos(w_{cj} t + \theta_j)\right) + n_i(t) \quad (21)$$

where $i = 1, 2, 3, \ldots, N$.

### 5.1 Maximum ratio combining

The MRC combiner weights each output signal $\{i_{ri}(t)\}_{i=1}^N$ from each link by gain $\{a_i\}_{i=1}^N$ proportional to the received intensity. The weighted signals are then co-phased and coherently added to obtain the combiner output current (22). In the absence of interference MRC is the optimal, regardless of the fading statistics, as it results in a maximum-likelihood receiver [21]. However, the performance superiority of MRC comes with a price of complexity as it clearly requires the knowledge of the received intensity on each link in addition to the subcarrier phase estimates required for the coherent summation

$$i_{\mathrm{MRC}}(t) = \sum_{i=1}^{N} a_i i_{ri}(t) \quad (22)$$

The optimum combiner output $\mathrm{SNR_e}$ $\gamma_{\mathrm{MRC}}$ obtained after filtering out the DC component is given as

$$\gamma_{\mathrm{MRC}} = \left(\frac{RA}{\sqrt{2N}}\right)^2 \sum_{i=1}^{N} \frac{I_i^2}{\sigma^2} = \sum_{i=1}^{N} \gamma_i \quad (23)$$

where $\gamma_i = (RAI_i/\sqrt{2N}\sigma)^2$ is the SNR for each link.

The unconditional BER with MRC is obtained by averaging the conditional error rate over the statistics of the intensity fluctuation across all the links, which is given as

$$P_{\mathrm{e(MRC)}} = \int_0^\infty Q\left(\sqrt{\gamma_{\mathrm{MRC}}}\right) P_I(I)\, \mathrm{d}I \quad (24)$$

where $P_I(I)$ is the joint pdf of scintillation given by (25) for receivers with spatial separation $s > \rho_o$

$$P_I(I) = \prod_{i=1}^{N} P_{I_i}(I_i) \quad (25)$$

Solving (24) involves $(N+1)$-fold integration if the classical definition of the $Q$-function is used. But using the alternative form of the $Q$-function and the Gauss–Hermite quadrature integration described in Section 4.2, (24) is reduced to that an equation involving single integration

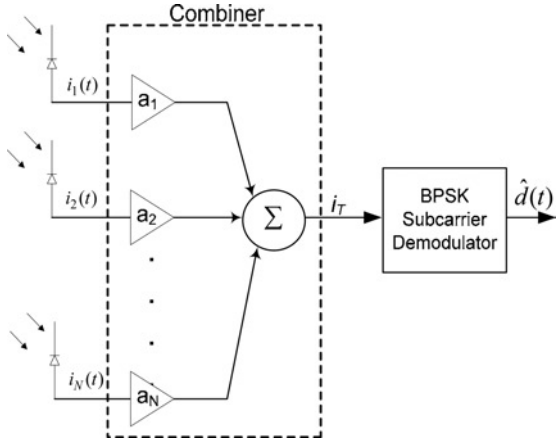


**Fig. 4** *Spatial diversity receiver with N-detectors*

$$P_{\mathrm{e(MRC)}} = \frac{1}{\pi} \int_0^{\pi/2} [S(\theta)]^N \mathrm{d}\theta \quad (26)$$

where $S(\theta) \simeq 1/\sqrt{\pi} \sum_{j=1}^{m} w_j \exp(-(K_0^2/2\sin^2\theta) \exp[2(x_j\sqrt{2}\sigma_l - \sigma_l^2/2)])$ and $K_0 = RI_0A/\sqrt{2N}\sigma$. With $N = 1$, (26) unsurprisingly gives the same result as in (20).

### 5.2 Equal gain combining

In EGC, the diversity combiner collates the photocurrents $\{i_{ri}(t)\}_{i=1}^N$, extracts each photocurrent phase estimate and sums them coherently with equal weights of unity [21]. The combined output photocurrent with the DC component filtered out is given by

$$i_{\mathrm{EGC}}(t) = \sum_{i=1}^{N} \left[\frac{R}{N} I_i \sum_{j=1}^{M} A_j g(t) \cos(w_{cj} t + \theta_j)\right] + n(t) \quad (27)$$

The $\mathrm{SNR_e}$ at the output of the EGC combiner conditioned on the received signal intensity is given as

$$\gamma_{\mathrm{EGC}} = \frac{(RA/\sqrt{2}N)^2 (\sum_{i=1}^{N} I_i)^2}{\sigma^2} \quad (28)$$

We assumed the sum of $N$ log-normal random variables to be another log-normal random variable $Z = \mathrm{e}^U$, where $U \sim N(\mu_u, \sigma_u^2)$ [13] and did not use the central limit theorem as the number of receivers $N$ under consideration is relatively small ($N \leq 10$). Parameters of $U \sim N(\mu_u, \sigma_u^2)$ are defined in (30). We therefore derived the unconditional BER by using the approach described in Section 4.2 as

$$\begin{aligned} P_{\mathrm{e(EGC)}} &= \int_0^\infty Q(\gamma_{\mathrm{EGC}}) P_I(I) \mathrm{d}I \\ &= \int_0^\infty \frac{1}{\pi} \int_0^{\pi/2} \exp\left(-\frac{K_1^2}{2\sin^2(\theta)} Z^2\right) P_Z(Z)\, \mathrm{d}\theta\, \mathrm{d}Z \\ &= \frac{1}{\sqrt{\pi}} \sum_{i=1}^{m} w_i Q(K_1 \mathrm{e}^{(x_i\sqrt{2}\sigma_u + \mu_u)}) \end{aligned} \quad (29)$$

where $P_I(I)$ represents the joint pdf of scintillation, $K_1 = RI_0A/\sqrt{2}\sigma N$, $P_z(Z) = (1/\sqrt{2\pi}\sigma_u)(1/Z) \exp\{-(\ln Z - \mu_u)^2/2\sigma_u^2\}$. $w_i$ and $x_i$ are defined earlier. With only one

receiver, (29) gives the same expression as (20)

$$\mu_u = \ln(N) - \frac{1}{2}\ln\left(1 + \frac{e^{\sigma_l^2} - 1}{N}\right)$$
$$\sigma_u^2 = \ln\left(1 + \frac{e^{\sigma_l^2} - 1}{N}\right) \quad (30)$$

### 5.3 Selection combining

Here, the combiner samples all $i_r(t)$ and selects the link with the highest SNR (or signal strength because all the branches are assumed to have the same noise level) without the need to estimate the phase of every $i_r(t)$. It is therefore of lower complexity when compared with MRC and EGC. The pdf of the received intensity $I = \max(I_1, I_2, \ldots, I_N)$ is obtained by first obtaining its cumulative density function and then taking the derivative. With the assumption of independent and identically distributed intensity, the pdf is derived as

$$p(\max(I_1, I_2, \ldots, I_N)) = \frac{2^{1-N} N \exp(-y^2)}{I\sigma_l\sqrt{2\pi}} \times [1 + erf(y)]^{N-1} \quad (31)$$

where $y = (\ln(I/I_0) + \sigma_l^2/2)/\sqrt{2}\sigma_l$.

The following gives the unconditional BER derived by combining the alternative form of $Q$-function with the Gauss–Hermite quadrature integration

$$P_{e(SelC)} = \frac{2^{1-N} N}{\sqrt{\pi}} \sum_{i=1}^{m} w_i [1 + erf(x_i)]^{N-1} \times Q\left(K_0 \exp\left(\frac{x_i\sqrt{2}\sigma_l - \sigma_l^2}{2}\right)\right) \quad (32)$$

where $K_0 = RI_0A/\sqrt{2N}\sigma$.

### 5.4 Results and discussions

Table 1 gives the parameters and their values used for the numerical simulation. In all our plots, the electrical SNR is normalised as $(RE[I])^2/\sigma^2$. Following the fact that the expressions derived thus far are for the BER on each subcarrier, we therefore define the overall BER for $M$-multiple SIM system as $1/M\sum_{i=1}^{M} P_{ei}$. This is same as the BER $P_e$ on each subcarrier as all the subcarriers are BPSK-modulated.

*5.4.1 No diversity:* In Fig. 5, the performance superiority of subcarrier modulation in a turbulent atmosphere is made evident, with the SNR required by SIM normalised by that

**Table 1: Numerical simulation parameters**

| Parameter | Symbol | Value |
|---|---|---|
| Turbulence level | $\sigma_l^2$ | $0.2^2 \le \sigma_l \le 1$ |
| Normalised received intensity with no turbulence | $I_0$ | 1 |
| Modulation index | $\beta$ | 1 |
| Number of uncorrelated receivers | $N$ | $1 \le N \le 10$ |
| Order of Hermite polynomial | $m$ | 20 |
| Mean received intensity | $E[I]$ | $I_0$ |
| Photodetector responsivity | $R$ | 1 |

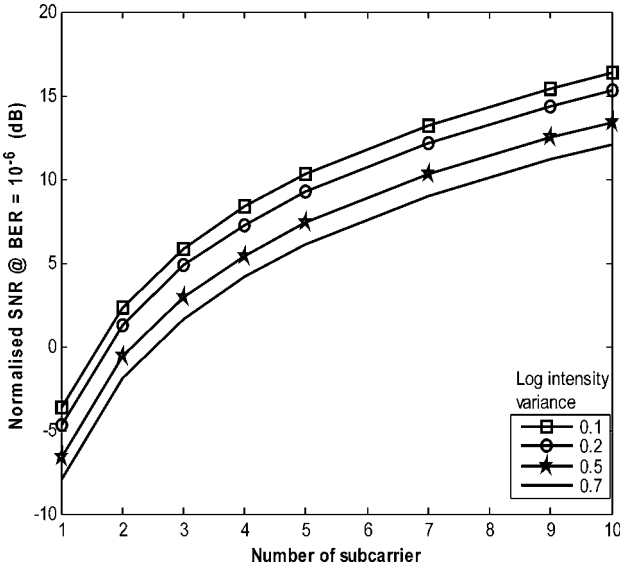


**Fig. 5** *Normalised SNR at BER of $10^{-6}$ against the number of subcarriers for various turbulence levels*

of OOK at the specified BER. The dependence of OOK optimum threshold level on turbulence is illustrated in Fig. 1 of Section 3; as turbulence level (log intensity variance) decreases, the threshold level approaches the halfway mark. At such instances, the performance superiority in terms of SNR of single subcarrier BPSK-modulated FSO over OOK tends towards the 3 dB expected in the absence of turbulence. However, as the turbulence level increases, the OOK threshold level drops rapidly from the halfway mark and therefore the single subcarrier BPSK-modulated FSO link becomes more superior when compared with OOK (Fig. 5). This result can be attributed to the fact that in OOK, the received irradiance directly represents digital information and any fluctuation in the irradiance directly impacts on the error probability. In subcarrier modulation, however, the data are hidden in the subcarrier phase. The extra margin in SNR could be used to either increase the number of subcarriers (thereby increasing the throughput) or increase the link range. Depending on the turbulence level up to about three subcarriers can be accommodated using the same SNR required by OOK to achieve BER of $10^{-6}$; translating into about triple the OOK throughput, provided each subcarrier carries same data rate as the OOK.

The SNR required for a given BER increases as the turbulence increases, as shown in Fig. 6. For an increase in turbulence from $\sigma_l = 0.1$ to 0.7, the SNR required to achieve a BER of $10^{-6}$ increased by $\simeq$20 dB, irrespective of the number of subcarriers. However, for a given turbulence level, the required SNR to achieve a BER of $10^{-6}$ increases with the number of subcarriers, as shown in Fig. 6.

*5.4.2 Spatial diversity:* Having shown in the previous section that without diversity, SIM outperforms optimum OOK and that multiple SIM is only suitable when increased capacity is of greater importance because it results in increased SNR (Fig. 6), we limit our discussion to single subcarrier SIM with spatial diversity. Denoting the SNR to achieve a BER of $10^{-6}$ with $N$ detectors at turbulence level $\sigma_l$ by $\gamma_{N,\sigma_l}$ and the spatial diversity gain by $m_{N,\sigma_l} = \gamma_{1,\sigma_l} - \gamma_{N,\sigma_l}$ (i.e. the ratio of SNR without diversity to that with spatial diversity at a given turbulence level), we plotted in Figs. 7 and 8 the spatial diversity gain $m_{N,\sigma_l}$ against $N$ for different levels of turbulence. $\gamma_{N,\sigma_l}$ and $\gamma_{1,\sigma_l}$ values were obtained from the separate plots of (26), (29) and

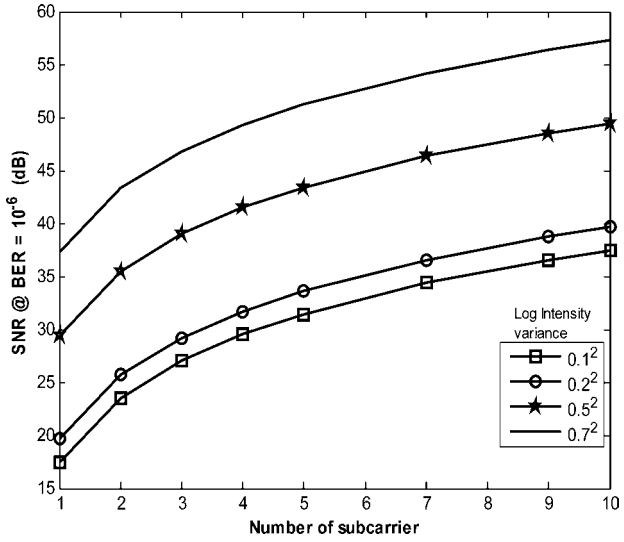


**Fig. 6** *SNR at BER of $10^{-6}$ against number of subcarrier for various turbulence levels with one photodetector*

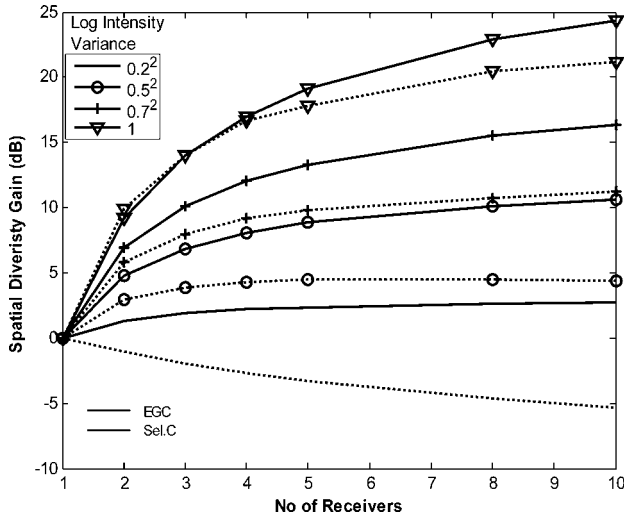


**Fig. 7** *Spatial diversity gain with EGC and SelC against the number of receivers for various turbulence levels*

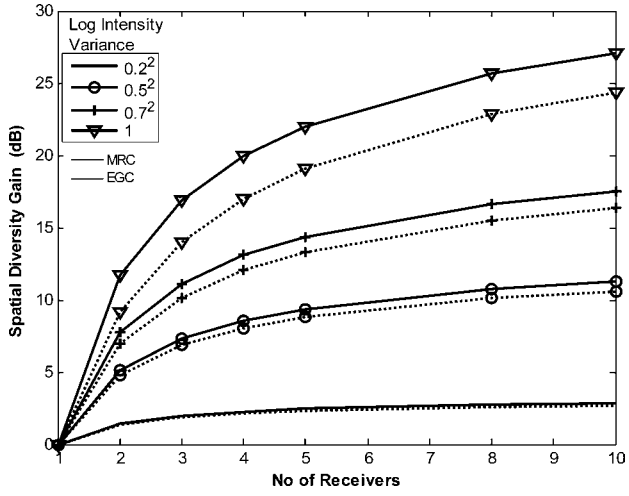


**Fig. 8** *Spatial diversity gain with EGC and MRC against the number of receivers for various turbulence levels*

(32). Fig. 7 shows that for $\sigma_l = 0.2$, the spatial diversity with SelC is poorer than when no diversity is used, thus resulting in up to $-5$ dB diversity gain. This can be ascribed to the fact that at very low turbulence, the effect of reducing the intensity received by factor $N$ on each link is dominant over the turbulence-induced intensity fluctuation. However, as the turbulence increases, selection diversity starts to payoff, but the performance is still inferior to that of EGC. We will therefore not suggest the use of solely SelC spatial diversity as a way of mitigating the effect of turbulence.

The phenomenal spatial diversity gain obtained from MRC and EGC spatial diversity is depicted in Fig. 8, where EGC diversity gain is between 0 and $\sim$2 dB (depending on the turbulence severity), lower than that of the complex MRC. Over the range of turbulence levels $0.2 \leq \sigma_l \leq 1$, the theoretical spatial diversity gain with two photodetectors employing MRC is $\sim 2 \leq m_{2,\sigma_l}(\text{dB}) \leq \sim 12$ and this increases to $\sim 2 \leq m_{4,\sigma_l}(\text{dB}) \leq \sim 20$ with four detectors. Another inference from the plots is that spatial diversity gain (link margin) becomes more pronounced as scintillation increases; using two detectors with MRC at a turbulence level of $\sigma_l = 0.2$ gives a diversity gain which is $\simeq$10 dB less than at $\sigma_l = 1$. Also, for $N \geq 4$, the marginal spatial diversity per unit detector $(m_{N,\sigma_l} - m_{N-1,\sigma_l})$ reduces drastically as the graphs start to flatten out. For instance, increasing $N$ from 4 to 10 with MRC across turbulence levels $0.2 \leq \sigma_l \leq 1$ only resulted in a marginal increase of between 0 and $\sim$6 dB diversity gain, whereas increasing $N$ from 1 to 4 resulted in an increase of between $\sim$3 and $\simeq$22 dB. Conversely, both the complexity and manufacturing cost increase significantly as the number of receivers $N$ is increased. We therefore suggest a reasonable number of detectors to mitigate turbulence without overwhelming complexity to be $2 \leq N \leq 4$.

## 6 Conclusion

Maximum ratio combining, EGC and SelC spatial diversity techniques have been applied to subcarrier intensity-modulated FSO under weak atmospheric turbulence, with BER expression derived for each. The use of SelC has shown to result in the lowest spatial diversity gain of all the techniques. For $\sigma_l \leq 0.2$, it was shown that adopting no diversity will result in improved performance, compared with SelC. As such, SelC is not suggested as the sole means of mitigating scintillation.

Compared with MRC, the EGC link margin is lower by up to 2 dB depending on turbulence severity. We have also shown that for BER of $10^{-6}$ single subcarrier modulation requires up to 7 dB (depending on turbulence severity) less SNR compared with the OOK. This extra margin may be used to increase either the throughput or the link span. A significant spatial diversity gain of up to $\sim$22 dB can be obtained by using up to four independent receivers with MRC. This clearly demonstrates the potency of spatial diversity in mitigating scintillation more so that the photodetectors receive uncorrelated irradiance. Our spatial diversity gain results are similar in trend to that reported in an earlier work by Lee and Chan [13] in which the outage probability is considered on binary pulse position modulation as the performance metric.

We have also shown that as the scintillation level rises, spatial diversity offers increased link margin. However, increasing the number of receivers beyond four only increases the system complexity and cost, but does not lead to a proportionate increase in the link margin. Moreover, from the results, EGC performance is slightly inferior to MRC but is far less complex to implement, and it is therefore

recommended as a spatial diversity combining technique for mitigating scintillation effects on terrestrial FSO.

## 7 Acknowledgment

This research is partly funded by the British Government under the ORSAS and Northumbria University at Newcastle upon Tyne, UK

## 8 References

1 Willebrand, H., and Ghuman, B.S.: 'Free space optics: enabling optical connectivity in today's network' (SAMS publishing, Indiana, 2002)
2 Kedar, D., and Arnon, S.: 'Optical wireless communication through fog in the presence of pointing errors', *Appl. Opt.*, 2003, **42**, pp. 4946–4954
3 Kamalakis, T., Sphicopoulos, T., Sheikh Muhammad, S., and Leitgeb, E.: 'Estimation of power scintillation statistics in free space optical links using the multi canonical Monte Carlo method'. IEEE Int. symp. on communication systems, networks and digital signal processing (CSNDSP, 2006), July 2006, Patras, Greece, pp. 629–633
4 Li, J.T., and Uysal, M.: 'Optical wireless communications: system model, capacity and coding', *Vehicular Technol. Conf.*, 2003, **1**, pp. 168–172
5 Uysal, M., Li, J.T., and Yu, M.: 'Error rate performance analysis of coded free-space optical links over gamma-gamma atmospheric turbulence channels', *IEEE Trans. Wireless Commun.*, 2006, **5**, pp. 1229–1233
6 Korevaar, E., Kim, I.I., and McArthur, B.: 'Atmospheric propagation characteristics of highest importance to commercial free space optics', MRV Communications white paper: available at http://www.mrv.com/library/library.php?view=wp. Accessed July 2007
7 Pratt, W.K.: 'Laser communication systems' (John Wiley & Sons, Inc., New York, 1969, 1st edn.)
8 Gagliardi, R.M., and Karp, S.: 'Optical communications' (New York, John Wiley, 1995, 2nd edn.)
9 Bloom, S., Korevaar, E., Schuster, J., and Willebrand, H.: 'Understanding the performance of free-space optics', *J. Opt. Netw.*, 2003, **2**, pp. 178–200
10 Zhu, X., and Kahn, J.M.: 'Free-space optical communication through atmospheric turbulence channels', *IEEE Trans. Commun.*, 2002, **50**, pp. 1293–1300
11 Ohtsuki, T.: 'Multiple-subcarrier modulation in optical wireless communications', *IEEE Commun. Mag.*, 2003, pp. 74–79
12 Djordjevic, I.B., and Vasic, B.: '100-Gb/s transmission using orthogonal frequency -division multiplexing', *IEEE Photonics technol. lett.*, 2006, **18**, pp. 1576–1578
13 Lee, E.J., and Chan, V.W.S.: 'Optical communications over the clear turbulent channel using diversity', *IEEE J. Select. Areas Commun.*, 2004, **22**, pp. 1896–1906
14 Osche, G.R.: 'Optical detection theory for laser applications' (Wiley, New Jersey, 2002)
15 Goodman, J.W.: 'Statistical Optics' (John Wiley, New York, 1985)
16 Yuksel, H.: 'Studies of the effects of atmospheric turbulence on free space optical communications', in Electrical and Computer Engineering', PhD thesis, University of Maryland, 2005, College Park, USA
17 Proakis, J.G.: 'Digital communications' (McGraw-Hill, New York, 2004)
18 You, R., and Kahn, J.M.: 'Average power reduction techniques for multi-subcarrier intensity-modulated optical signals', *IEEE Trans. commun.*, 2001, **49**, pp. 2164–2171
19 Djordjevic, I.B., Vasic, B., and Neifeld, M.A.: 'LDPC coded OFDM over the atmospheric turbulence channel', *Opt. Express*, 2007, **15**, pp. 6336–6350
20 Teramoto, S., and Ohtsuki, T.: 'Multiple-subcarier optical communication systems with subcarrier signal-point sequence', *IEEE Trans. Commun.*, 2005, **53**, pp. 1738–1743
21 Simon, M.K., and Alouini, M.S.: 'Digital communication over fading channels' (John Wiley & Sons Inc., 2004, 2nd edn.)
22 Abramowitz, M., and Stegun, I.S.: 'Handbook of mathematical functions with formulars, graphs and mathematical tables' (Dover, 1977)